Development of a Volkswagen Jetta MK5 Hybrid Vehicle for Optimized System Efficiency Based on a Genetic Algorithm

Husam A. Neamah [1,2,*], Mohammed Dulaimi [3], Alaa Silavinia [1], Aminu Babangida [1]
and Péter Tamás Szemes [1]

1   Department of Electrical Engineering and Mechatronics, Faculty of Engineering, University of Debrecen,
     Ótemető Utca 2-4, 4028 Debrecen, Hungary; alaa@mailbox.unideb.hu (A.S.);
     aminu.babangida@eng.unideb.hu (A.B.); szemespeter@eng.unideb.hu (P.T.S.)
2   Technical Engineering College, Al-Ayen University, Thi-Qar 64001, Iraq
3   College of Engineering, University of Warith Al-Anbiyaa, Karbala 56001, Iraq;
     mohammed.dekan@uowa.edu.iq
*   Correspondence: husam@eng.unideb.hu

Abstract: Hybrid electric vehicles (HEVs) have emerged as a trendy technology for reducing over-dependence on fossil fuels and a global concern of gas emissions across transportation networks. This research aims to design the hybridized drivetrain of a Volkswagen (VW) Jetta MK5 vehicle on the basis of its mathematical background description and a computer-aided simulation (MATLAB/Simulink/Simscape, MATLAB R2023b). The conventional car operates through a five-speed manual gearbox, and a 2.0 TDI internal combustion engine (ICE) is first assessed. A comparative study evaluates the optimal fuel economy between the conventional and the hybrid versions based on a proportional-integral-derivative (PID) controller, whose optimal set-point is predicted and computed by a genetic algorithm (GA). For realistic hybridization, this research integrated a Parker electric motor and the diesel engine of a VW Crafter hybrid vehicle from the faculty of engineering to reduce fuel consumption and optimize the system performance of the proposed car. Moreover, a VCDS measurement unit is developed to collect vehicle data based on real-world driving scenarios. The simulation results are compared with experimental data to validate the model's accuracy. The simulation results prove the effectiveness of the proposed energy management strategy (EMS), with an approximately 89.46% reduction in fuel consumption for the hybrid powertrain compared to the gas-powered traditional vehicle, and 90.05% energy efficiency is achieved.

Keywords: drivetrain; genetic algorithm (GA); internal combustion engine (ICE); 1.9 TDI PD engine; 2.0 TDI CR diesel engine

1. Introduction

1.1. Background

The global usage of hydrocarbon-based transportation has resulted in several issues, including an increased need for petroleum production, rising fuel costs, and climate change. Transportation and environmental researchers are actively pursuing alternative, efficient, reliable, and ecological solutions to these problems. HEVs have been adopted to address these negative trends.

Gas-powered vehicles, either using gasoline or diesel as a fuel, have been used for decades. They are also known as internal combustion engine vehicles. They convert the energy from burning the fuel into mechanical energy to power the car. They are known as a prime source of carbon dioxide (CO_2) emissions, which cause global warming [1,2], nitrogen oxides (NO_x), unburned hydrocarbons (HC), and carbon monoxide (CO) [3]. Moreover, the drawback of such vehicles is that ICEs have low efficiency compared to electrical motors, which have an efficiency of about 85% [4]. The low efficiency of the ICE and its transient response eventually cause the traditional gas-powered cars to have a

poor fuel economy [5,6]. These problems highlight the need for alternative and sustainable solutions in the transportation sector, such as electric and autonomous vehicles, air-powered engines, and exhaust gas engines, to mitigate the environmental and energy-related issues associated with gas-powered vehicles [7,8].

In recent years, the automotive industry has striven towards the adaptation of hybrid powertrain propulsion to reduce the widespread concern about environmental emissions and fossil fuel consumption. Therefore, in the context of the current global trend of dangerous air pollutant emissions, and to decrease the demand for fossil fuels, research activity must develop cleaner alternatives from renewable sources and HEVs [9]. The importance of achieving a zero-emissions environment is emphasized in light of the environmental challenges posed by the automobile industry, especially the depletion of vital resources and greenhouse gas emissions contributing to climate change. Electric vehicles (EVs) and HEVs emerge as viable solutions, reducing emissions and reliance on energy resources. Electric cars, especially those that use High-Temperature Superconductor (HTS) technology in their electric motors, show the potential to surpass conventional combustion vehicles. This technology conserves and facilitates adequate torque generation in EVs. Furthermore, the widespread adoption of EVs and HEVs promises significant reductions in gas emissions [10,11]. From a research perspective, HEVs have received serious attention across the scientific community.

In many domains, from industrial operations to renewable energy systems, optimal energy management is fundamental. Control techniques are required for the best possible energy management, because they enable resource conservation and practical use. The linear control method, modeled by the proportional integral derivative (PID) [12], was adopted for energy management in HEVs. The controller balances power distribution between the ICE and the electric motor. The operation of the PID was studied in Ref. [13]. However, the PID may not guarantee an optimal performance, because it requires a precise mathematical model of the system.

Recently, another popular control method, adaptive control, was adopted. Adaptive control represents a sophisticated approach that dynamically changes the control characteristics. According to [14], adaptive control techniques are robust due to dynamic changes in driving conditions in hybrid vehicles. These techniques can dynamically tune control parameters in response to changes in vehicle operating conditions, thereby optimizing energy consumption and accuracy. A model predictive controller (MPC) is another promising controller applied for optimal fuel consumption for HEVs. In Ref. [15], various literature studies were performed for a MPC as an alternative and valuable energy management strategy in HEVs. However, optimal performance could not be guaranteed if there were poor predictions. In Ref. [16], a fuzzy logic controller (FLC) was proposed for optimal fuel economy in a parallel HEV. The simulation results show that the FLC is also a promising technique. The FLC is indeed a powerful control tool suitable for nonlinear systems [17]. Moreover, a fractional order proportional-integral-derivative (FOPID) controller has also been proposed as a promising technique, as in Ref. [18].

The broader application of HEVs has led to the development of more advanced control techniques and optimization methods for optimal fuel economy. An EMS is an integral part of the vehicle. The EMS is divided into optimization-based and rule-based methods. Optimization-based methods have received wider attention in the context of scientific manuscripts. However, in Ref. [19], the rule-based method uses pre-defined rules to determine when to switch between engines and electric motors considering speed, load, and battery status. In [1], an advanced RBC strategy based on machine learning was proposed to develop the mode control map. This technique includes reinforcement learning and neural networks. These methods can be adapted to different driving conditions and learn from historical data. Machine learning-based controller methods can optimize power sharing based on complex nonlinear relationships.

A significantly greater focus has been placed on GAs on a global scale, according to the study introduced in Ref. [20]. Incorporating artificial intelligence technology and the mechanism of biological evolution into optimization approaches, a distinct set of methods

has emerged [20]. These methods deviate significantly from traditional optimization techniques, providing a fresh perspective on modern methods [21].

Inspired by the above, this research proposes an enhanced PID control-based GA to compute the optimal fuel economy of the developed Jetta MK5 vehicle. The GA within evolutionary computing has gained considerable attention among contemporary optimization algorithms. This is attributed to its effective global search capabilities and the inherent advantage of low algorithmic complexity.

1.2. Establishment of Jetta MK5 Vehicle

The Volkswagen Jetta MK5 is a compact vehicle manufactured by the German automaker Volkswagen. In production from 2005 to 2010, this generation showcased a contemporary and refined design compared to its forerunner, emphasizing enhanced interior quality and comfort [22].

Aligned with the Golf MK5, it shared a platform and offered various engines, encompassing petrol, diesel, and turbocharged alternatives. The vehicle's energy consumption, intrinsically linked to fuel efficiency, varied across the engine options available in the MK5 Jetta, which comprised gasoline, diesel, and turbocharged variants. Some factors influencing fuel efficiency included engine size, transmission type, and driving conditions [22]. Table 1 shows the general technical specifications of the vehicle. A 2.0 TDI engine is used in this research. It uses a DPF combined with diesel exhaust fluid (DEF) and is characterized by high output torque, reduced fuel consumption, and lower emissions. Additionally, Table 2 presents the parameters used in this research's simulation aspect. The curb weight is considered in this research, since the experimental aspect does not take into account the gross weight of the vehicle.

Table 1. Jetta MK5 vehicle's main technical specifications [23].

Parameters	Specifications
Length	4.554–4.556 m
Width	1.781 m
Height	1.459–1.504 m
Tract, front	1.534–1.541 m
Tract, rear	1.512–1.514 m
Wheelbase	2.578 m
Curb weight	1268–1650 kg
Gross weight	1870–2030 kg
Chassis construction	Unibody
Engine displacement	1968 cc (120.1 cu in)
Number of strokes	4
Number of cylinders	4
Fuel system	Common rail
Bore x stroke	0.081×0.0955 m
Number of valves	16
Compression ratio	16.2:1
After treatment systems	Diesel Particulate Filter (DPF)
Tire radius	225/45 R17 (0.4318 m)

Table 2. Vehicle body parameters and specifications [23].

Parameters	Specifications
Curb weight of the vehicle	1268 kg
Gross weight of the vehicle	1870 kg
Center of gravity height	0.486 m
Tract, front	1.534 m
Tract, rear	1.512 m
Rolling resistance coefficient	0.012
Coefficient of aerodynamic resistance	0.3
Atmospheric density	1.225 kg/m^3
Gravitational force	9.81 m/s^2
Front area	2.209 m^2

1.3. Establishment of 2.0 TDI Diesel ICE

The 2.0 TDI or 2.0 Turbocharged Direct Injection is an internal combustion diesel engine that provides excellent fuel economy and efficiency. The engine uses direct fuel injection in the combustion chamber to increase combustion efficiency and overall performance. This technology is known for providing operating power and balanced fuel use [24].

An additional consideration in evaluating the MK5 Jetta pertained to potential issues, such as fuel system complications, particularly fuel pump failures, which had the potential to disrupt fuel delivery, thereby influencing energy consumption. Diesel models have faced concerns relating to the Diesel Particulate Filter (DPF), impacting engine performance and fuel efficiency [24]. Additionally, problems with the electrical system could affect sensors and engine management, thereby influencing fuel injection and combustion efficiency. Table 3 presents the parameters of the engine used in the new design of our vehicle.

Table 3. PMSM parameters and specifications.

Parameters	Specifications
Motor power	103 kW
Motor torque	400 Nm
Torque control time constant	0.02 s
External series resistance	0
Inertia of the rotor	3.9×10^{-4} kg m^2
Damping of rotor	10^{-5} Nm/[rad/s]

1.4. Research Aim, Objectives, and Contributions

This research aims to design an optimal EMS system based on an enhanced PID controller for a VW Jetta MK5 vehicle, and the specific objectives are as follows: 1. to design a conventional and parallel plug-in hybrid electric vehicle (PHEV) version of the VW Jetta MK5; 2. to perform a comparative study based on the optimal fuel economy between the proposed car's conventional and hybrid versions; 3. to assess the simulated model's performance by comparing the real measurement data for the proposed vehicle with the help of VCDS software (VCDS Release 20.4.2). The main contributions of this paper are as follows: 1. A meta-heuristic method (GA algorithm) for the EMS of the PHEV is proposed to achieve minimization of the fuel economy by 89.46%. 2. The 2.0 LTDI CR diesel engine replaces the older version of this vehicle's 1.9 L TDI PD diesel ICE for better performance. 3. The study successfully transforms the conventional version of the VW Jetta MK5 vehicle into a hybrid.

The remaining part of this paper is structured as follows: Section 2 presents a description of the mathematical background of the vehicle dynamics system, the battery, the electric motor, and the diesel engine. Section 3 gives the control design description and optimization. Section 4 introduces the VCDS unit and the data collection approach. Section 5 presents the MATLAB (MATLAB R2023b) models. Section 6 presents the simulation and experimental results. Section 7 discusses and describes the qualitative and quantitative findings. Section 8 gives the conclusion.

2. Mathematical Modeling

2.1. Vehicle Dynamics

The vehicle's motion caused by the steering movement, through which the car is capable of autonomous motion, is referred to as vehicle dynamics [25]. A vehicle's dynamic is divided into longitudinal, lateral, and vertical dynamics. Using the longitudinal dynamic, we modeled the vehicle on a MATLAB/Simulink/Simscape (MATLAB R2023b) environment. In real life, a car travels not just on level ground but also up and down hills, through turns, and on slopes [26]. The longitudinal direction is simply the forward-moving direction of the vehicle, and there are two distinct perspectives on the forward path: one concerns the vehicle body directly, and the other concerns a fixed reference point. The

first is used when dealing with the acceleration and velocity of the vehicle, and the second is typically used when knowing where the car is in relation to a beginning or ending point, which is essential [27]. Figure 1 shows the forces operating on the vehicle using a fundamental free body diagram.
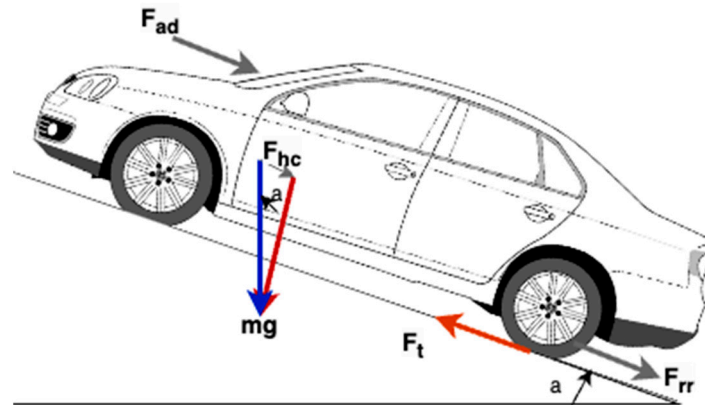

Figure 1. Free body diagram of the vehicle dynamics.

The vehicle characteristics using the free body diagram in Figure 1 and the tractive forces acting on the chassis or structure of the body are expressed in [28,29].

$$F_t = F_{ad} + F_{rr} + F_{hc} + F_A \tag{1}$$

$$Fad = 0.5\,\rho C_d A_f V^2 \tag{2}$$

$$F_{rr} = w\,C_{rr}cos\alpha \tag{3}$$

where F_{ad} is the air resistance, ρ is the air density, A_f is the frontal area, C_d is the drag coefficient, V is the vehicle speed, F_{rr} is the rolling resistance, which is determined by the vehicle's weight w (w = mg), and C_{rr} is the rolling resistance coefficient, a function of the rolling force and the normal force exerted by the tire on the road, as represented by Equation (3).

By implementing the equations based on the free body diagram, the following formulas were used for the forces brought about by resistance to the slope and the acceleration resistance:

$$F_{hc} = \omega sin\alpha \tag{4}$$

$$F_A = m_i a \tag{5}$$

where $m_i = 1.04\,m$ is the inertial vehicle mass, m represents the mass of the vehicle in kg, and *a* is the acceleration. The value 1.04 is an inertial mass factor assumed to account for the rotating inertia of the wheels and driveline. The following equations represent the energy and tractive power needed to move the vehicle:

$$P = FV \tag{6}$$

$$E = Pt \tag{7}$$

where *F* is the tractive force measured in newtons (N), and the time is measured in seconds (s).

Figure 2 depicts the modeling method and data analysis adopted in this research. The data were collected from a real Jetta MK5 vehicle with the help of VCDS software via an Onboard Diagnostic 2 (OBD2) interface connected to a PC (personal computer) using a hardware cable and MATLAB software for the visualization. The modeling approach was performed in two stages: Firstly, the ICE-powered version of the proposed vehicle was modeled in MATLAB, and the optimal fuel economy was computed and compared with the real measurement data. The 1.9 L TDI diesel engine of the older version of the car was replaced by the 2.0 L TDI diesel engine to improve the car's fuel economy, since the piston bore and the stroke ratio or displacement could affect the fuel economy. Another

critical factor to consider is better fuel delivery, not just peak pressure; however, this can be controlled by software, and the fuel timing will be handled in the broader domain. Secondly, the hybrid version of the car was modeled, and its optimal fuel economy was computed and compared with the conventional real and modeled car.
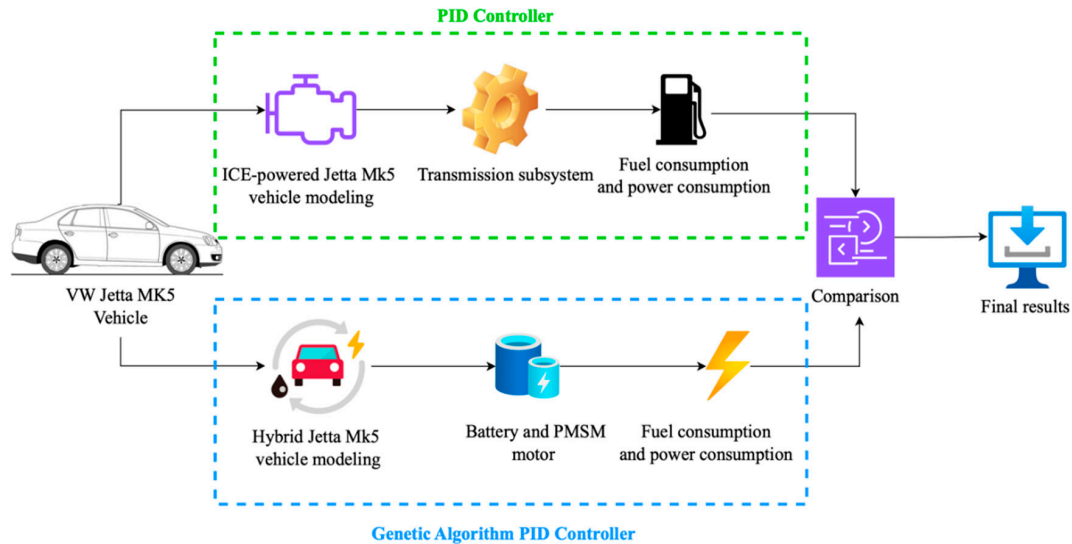

Figure 2. Modeling architecture and analysis.

2.2. Hybrid Powertrain Modeling

The mechanical connection mechanism connects the engine to the powertrain while the motor drives the vehicle. Depending on the load conditions, either an engine or a motor might power the car, significantly increasing fuel economy. When the vehicle is running at a lesser pace to save fuel, the motor supplies the power. Consequently, this system can maintain high performance and improve fuel consumption. The motor delivers power when the vehicle runs at low speeds to save fuel. The collective power is mechanical rather than electrical, and the engine and electric motor are connected to a gearset, chain, or belt, thus accumulating their torque and transmitting it to the wheels [30]. In this system, one of the electromechanical energy converters is identical. Parallel hybrid powertrains do not need to be sized to match the high-power requirements, but unless the electric motors are much larger, they carry less power than a series hybrid, because they do not get the total motor power, which lowers regenerative capacity and limits the usage of transmission systems to manually adjust brakes and other components based on engine speed. In addition, engine operational conditions are not as effectively controlled as they are in a series hybrid powertrains [30,31].

Figure 3 depicts the hybrid topology. Figure 4 shows the model-in-the-loop simulation of the hybrid vehicle in a MATLAB/Simulink environment.
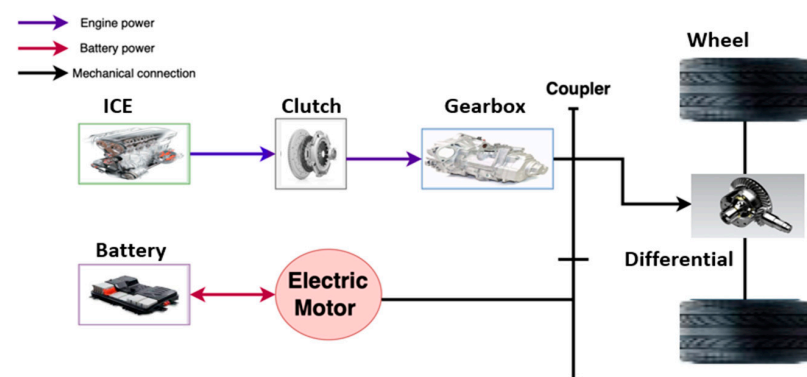

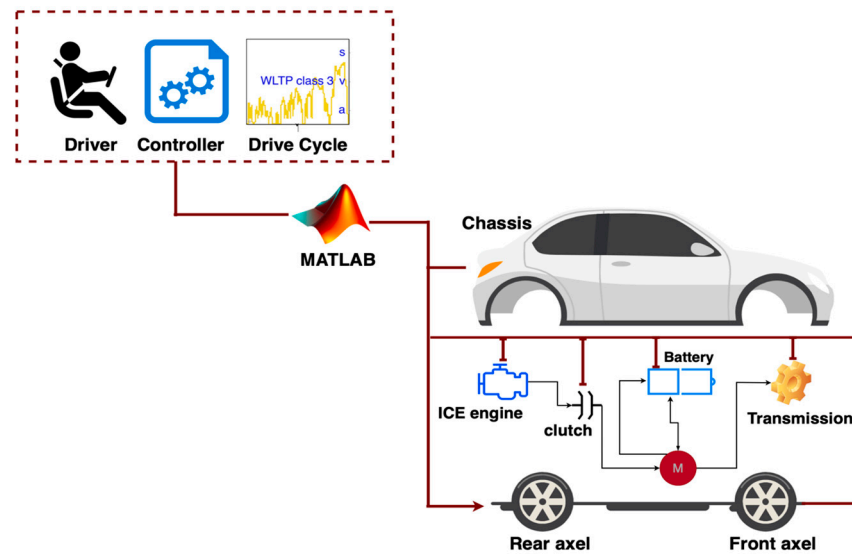**Figure 3.** Configuration of the hybrid powertrain.

Figure 4. Model-in-the-loop testing for the hybrid vehicle.

2.3. Battery Modeling

The battery's performance was analyzed quantitatively by employing an established equivalent circuit model sourced from the existing literature. This circuit, modeled after the Nissan Leaf, served as the foundation for our investigation and was subsequently built with the MATLAB-simulated built-in battery for comparative purposes. A 2011 Nissan Leaf battery with 360 V, 24 kWh rating is utilized in this research. The Nissan Leaf battery unit is made from 48 modules, each of which has four cells—two parallel and two series—for 192 cells. It is a lithium-ion battery with a 33.1 Ampere-hour (Ah) per cell capacity, giving the pack a maximum capacity of 66.2 Ah. The acceptable range for SOC_{bat} is from 0.2 to 1; falling below this interval decreases the battery's lifespan.

The voltage of the battery is given by

$$V_b = V_r^0 - \frac{RT}{nF}lnQ_R \tag{8}$$

Here, R represents the constant of gas, T stands for temperature, and Q_R stands for the reaction ratio, which varies with the level of the reacting substances. However, because every battery is coupled using an ohmic drop [32,33], it is possible to modify the equation as follows:

$$V_b = V_r^0 - \frac{RT}{nF}lnQ_R - R_b I_b \tag{9}$$

The following equation may then be modified to consider battery capacity as well:

$$V_b(I_b, y) = V_r^0 - Aln(By) - Ky - Fe^{G(y-y3)} - R_b I_b \tag{10}$$

where y is a variable relating to the battery's energy, capacity, SOC, or depth of discharge (DOD). The exponential fall begins at y_3, and the values obtained via a curve fitting are indicated by the letters A, B, K, F, and G. To convey the above equation in terms of DoD,

$$V_b(I_b, DoD) = V_r^0 - Aln(B\,DoD) - K\,DoD - Fe^{G(DoD-DoD_3)} - R_b I_b \tag{11}$$

The equations mentioned above can be used to simulate the corresponding circuit depicted in Figure 5. As a result, the previously described mathematical representation of the compact battery model, which rests on the integrated Simulink method, can convey the characteristics of the battery.
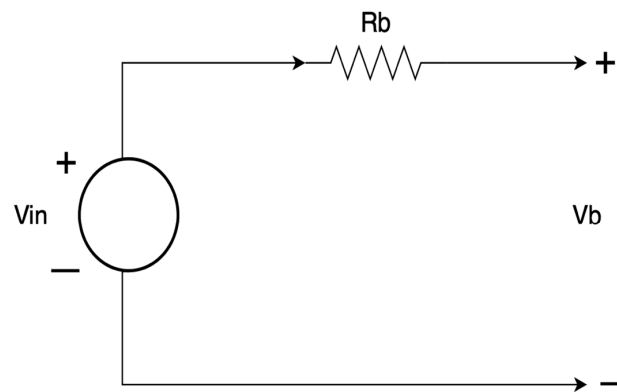
Figure 5. Simplified battery circuit [32].

However, the 2011 Nissan Leaf battery is proposed in this research due to its suitability for the proposed vehicle, especially when the range is the point of interest. "Recently, (in 2023) most of the PHEVs have an average of 22 kWh battery size, which would be more efficient, with extended range [34]. In August 2023, the average passenger EV sold globally, including BEVs, PHEVs and HEVs, had a battery capacity of 38.6 kWh, 9% higher than the same month a year ago [34]. BEVs had an average battery capacity of 62.5 kWh in August 2023 (up to 100 kWh can be used now for BEVs), which represents a less-than 1% increase over the previous month and an 8% leap compared to August 2022 [34]. PHEVs had an average battery capacity of 21.8 kWh in August 2023, an 8% expansion compared to July 2023 and a massive 27% capacity increase compared to last year [34]. HEVs had an average battery size of 1.3 kWh in August 2023, a slight increase over July 2023 and a 3% increase in capacity compared to August 2022 [34]".

2.4. PMSM Modeling

The PMSM used in the powertrain of the HEV model has advantages over other types of electric motors in EV applications. A permanent magnet installed on the rotor generates a spinning magnetic field, which produces a sinusoidal electromagnetic field [28].

The PMSM [35] mathematical model assumed the electromotive force (EMF) in the opposite direction was sinusoidal [28]. After a sinusoidal configuration, the magnetomotive force (MMF) is distributed in the airspace, and the position of the rotor limits the degree of salience. This concept ignores hysteresis and saturation by assuming a three-phase balanced supply voltage [36,37]. This determines the voltage of the three-phase power supply.

$$V_A = P\Psi_A + I_A R_S \qquad (12)$$

$$V_B = P\Psi_B + I_B R_S \qquad (13)$$

$$V_C = P\Psi_C + I_C R_S \qquad (14)$$

In the given context, I_A, I_B, and I_C signify the phase currents; V_A, V_B, and V_C are the phase voltages; Ψ_A, Ψ_B, and Ψ_C indicate the flux linkages; and R_S and P are the phase resistance and derivative operator, respectively [28,37]. Tables 3 and 4 present the specifications of the electric motor and the ICE.

Table 4. ICE parameters and specifications [38].

Parameters	Specifications
Engine power	81 kW
Engine torque	250 Nm
Engine time constant	0.01 s
External series resistance	0
Engine shaft inertia	0.25 kgm^2
Engine displacement	1968 cc
Number of cylinders	4, Inline
Transmission	5-speed, manual

A field-oriented controller (FOC) is a common control strategy for permanent-magnet synchronous motor PMSM drives. The FOC aims to control the motor currents by decoupling the torque and flow components, simplifying the control task, and allowing for precise motor control [39,40].

2.5. Engine Modeling

When the model parameterization is configured as a normalized third-order polynomial, the system utilizes the normalized engine speed, denoted as ω_N, for the calculation of both speed and torque [41]. The block specifies the normalized engine speed in Ref. [41] as follows:

$$\omega_N(\omega) = \frac{\omega}{\omega_{PP}} \tag{15}$$

where ω is the current engine speed, and ω_{PP} is the engine speed at peak power.

The model handles the normalized and dimensionless engine power as a third-order polynomial in such a way that

$$P(\omega(\omega_N)) = P_P \cdot p_N(\omega_N) \tag{16}$$

$$p_N(\omega_N) = s_1\omega_N + s_2\,\omega_N^2 + s_3\,\omega_N^3 \tag{17}$$

Here, s_1, s_2, and s_3 in Equation (17) represent the constant coefficients of a polynomial, and P_p denotes the peak power in Equation (16). In conventional engines, the coefficients are commonly positive. The module computes the engine torque under wide-open throttle conditions by employing these polynomial coefficients with the following expression [41]:

$$T(\omega(\omega_N)) = p_1 + p_2\omega_N + p_3\omega^2{}_N \tag{18}$$

$$p_1 = \frac{s_1 P_p}{\omega_{pp}} \tag{19}$$

$$p_2 = \frac{s_2 P_p}{\omega_{pp}} \tag{20}$$

$$p_3 = \frac{s_3 P_p}{\omega_{pp}} \tag{21}$$

The module configures the normalized engine speed to align with peak power, ensuring that

$$\omega_{NPP} = \omega_N(\omega_{NPP}) = 1 \tag{22}$$

The link between the torque of the engine (Q), the power generated (P), and the rotating speed (ω) can be presented by the following equation:

$$Q = \frac{P}{\omega} \tag{23}$$

The efficiency of the engine, labeled as η_f in Equation (24), is linked to the heating value Q_{hv} and the specific fuel consumption (SFC) as indicated by the given formulas. In [42], $\dot{m}_f$ is the mass flow rate for the fuel consumed, SFC is specific fuel consumption, and P is the power output as in Equation (26).

$$\eta_f = \frac{work\ output}{energy\ input} \times 100 \tag{24}$$

$$Q_{hv} = \frac{energy\ released\ during\ combustion}{Fuel\ mass} \tag{25}$$

$$SFC = \frac{\dot{m}_f}{P} \tag{26}$$

$$\eta_f = \frac{1}{SFC \cdot Q_{hv}} \tag{27}$$

For the partially opened throttle condition, the speed controller adjusts the throttle signal to increase the rotation of the engine below the desired speed according to Equations (28) and (29):

$$\Pi = max\ (\Pi_i, \Pi_c) \tag{28}$$

$$\frac{d(\Pi_c)}{dx} = \frac{0.5 \cdot \left(1 - tanh\left(4 \cdot \frac{\omega - \omega_r}{\omega_t}\right)\right) - \Pi_c}{\tau} \tag{29}$$

where Π is the throttle, Π_i is the input throttle, Π_c is the controller throttle, ω is the engine speed, ω_r is the partial or idle speed reference, ω_t is the controller speed threshold, and τ is the controller time constant [41].

2.6. Gearshift

A five-speed gearbox is designed for the proposed vehicle in this research, controlled with the help of a shift logic known as a gearbox controller in the MATLAB/Simulink environment. However, two common parameters are used to initiate the gearshift: the vehicle speed and the torque demand or throttle position [43]. The first gear ratio is fixed, and its selection is used to ensure enough hill capability to start the vehicle [44]. The vehicle's acceleration is assumed to be constant, with its lowest starting value in WLTP driving conditions. Let us assume no drag, no inertia effect, and an initial engine speed of 1000 rpm; then, the estimated ratio can be expressed as [44]

$$R_{first\ est.} = \frac{r_w m}{T_{eng.} \eta}(a_{WLTP} + gsin\theta_{max}) \tag{30}$$

The vehicle's velocity is calculated at the engine' speed of 1000 rpm as follows:

$$v = \frac{1000\pi r_w}{30R_{first\ est.}} \tag{31}$$

$$R_{first} = \frac{r_w}{T_{eng.}\eta_f}\left[a\left(m + \frac{I_{Eff}}{r_w^2}\right) + F_{ad} + F_{rr} + F_w\right] \tag{32}$$

where $R_{first\ est.}$ is the first estimated gear ratio, R_{first} is the first gear ratio, r_w is the tire radius, $T_{eng.}$ is the engine torque, a is the acceleration, m is the vehicle mass, and I_{Eff} is the inertia effect. This is repeated until the first gear converges [44]. However, the top gear (R_{top}) is expressed as [44]

$$R_{top} = \frac{2\pi r_w N_{Engmax}\ \eta_f}{60v_{motorway.}} \tag{33}$$

N_{Engmax} is the engine's maximum speed, and $v_{motorway}$ is the maximum motorway legal speed of the vehicle. However, the above formulations are used to optimize the gear ratios for the car from a theoretical point of view for two-speed transmission. This theoretical basis will be used in future research to optimize the five-speed gearbox.

Gearshift takes place based on some requirements. For example, a gear can be changed when the engine has reached a defined speed or if minimum emissions or fuel consumption is required [44]. Table 5 shows the gearshifts, ratios, and the clutch schedules (A, B, C, D, E) for the five-speed manual transmission used in this research. The gear ratios were adopted from Ref. [45].

Table 5. Clutch schedule and gearshift for the five-speed manual transmission.

Gearshift	Gear Ratio	A	B	C	D	E
First gear	3.778	1	0	0	0	0
Second gear	2.063	0	1	0	0	0
Third gear	1.360	0	0	1	0	0
Fourth gear	0.967	0	0	0	1	0
Fifth gear	0.769	0	0	0	0	1
Final drive	3.769	1	1	1	1	1

3. Control Design Description and Optimization

3.1. PID Controller Design

The PID controller is the most widely used control technique employed for industrial and mechatronics products due to its simplicity for practical implementation. In this research, a PID control optimized using a GA technique is designed as the EMS for the proposed vehicle. The controller consists of three terms: proportional gain (k_p), integral gain (k_i), and derivative gain (k_d). Each of these gains were used to provide the appropriate control action for optimal energy management for the vehicle. Reviewed literature works show that this control strategy's main task is to find an optimal value for the controller gains [46–48]. The operation of the PID used in this research is described with reference to Figure 6.
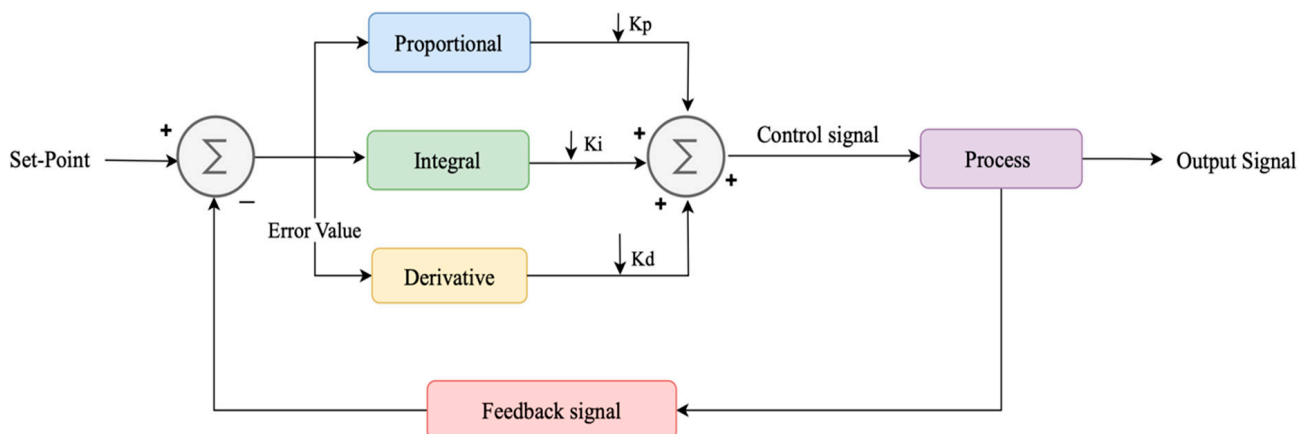
Figure 6. PID control action.

Therefore, the PID controller can be expressed mathematically as in Ref. [49] in Equation (34):

$$u(t) = k_p e(t) + k_i \int e(t) dt + k_d \frac{d}{dt} e(t) \tag{34}$$

The set-point is the reference vehicle speed in this research. The signal input to the PID controller is the difference [e.g., the speed error is $e(t)$] between the reference speed (drive cycle in km/h) and the vehicle's actual speed, also in km/h. In this way, the controller provides the appropriate signal to control the speed of the car. In addition, it gives the desired motor and engine speeds to produce the desired torque for propelling the vehicle's wheel. Therefore, the whole system model consisting of the battery, electric motor, and the vehicle systems has been linked to the optimization framework on the basis of the GA technique to reduce the vehicle's energy consumption.

3.2. Optimization of the PID Controller Using Genetic Algorithm

The purpose of using the GA to tune the PID controller is to minimize the cost of energy usage from the vehicle utilization. In Ref. [50], the most prevalent evolutionary algorithm solves optimization problems by keeping mechanisms spurred by natural changes such as

natural selection, inheritance, mutation, and crossover. The GA is used to select how the acquisition rate of the controller gains is optimized for our hybrid system. By minimizing the output response in relation to the oriented signal, the proposed controller attempts to decrease error. Physical characteristics for desired performance are often expressed in time field quantities [51].

The effectiveness of a control algorithm is ensured by the optimal selection of its tunning parameters. Therefore, the control parameters are on the basis of a defined objective function called performance indices, which should be minimized for optimized system performance [52]. Therefore, the use of a GA-PID energy management task is to be accomplished by defining the appropriate objective functions such as the Integral Squared Error (ISE), Integral Absolute Error (IAE), Integral of Time-weighted Absolute Error (ITAE), and the Integral of Time-weighted Squared Error (ITSE), where the squared error is temporally weighted before integration, like the ITAE criterion. The IAE and ISE formulae are used to create error criteria during the generation of the function. The suggested GA procedure developed in MATLAB can be summarized by defining the algorithm parameters in Table 6. Figure 7 shows how the GA is used to compute the optimal control gains for the whole system model to reduce fuel consumption.

Table 6. Genetic algorithm specifications.

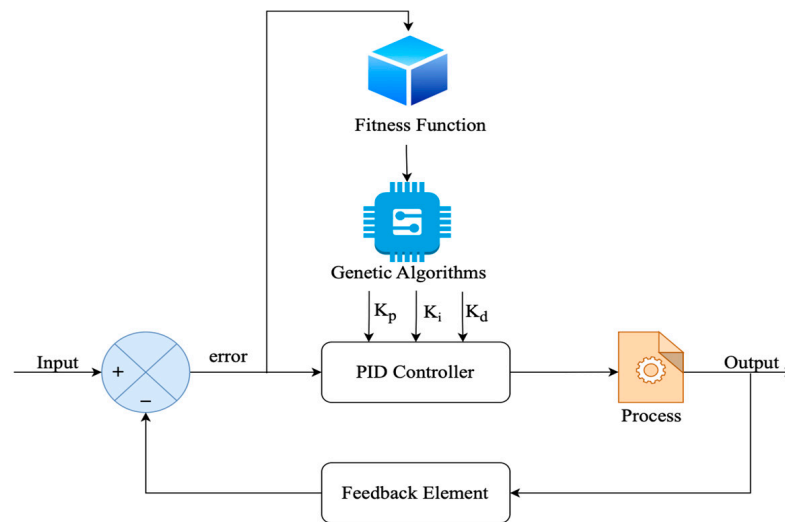| Execution of the Performance (FT)	Integral Error
Selection strategy	Random (cost function)
Generations	10
Population size	20
Fitness performance	proportional
Lower limit	[0 0 0]
Upper limit	[500 500 500]

Figure 7. GA-PID configuration.

However, given that $e(t)$ is the error at a time (t), and (T) is the total time of the simulation, the objective functions in terms of the errors are as follows:

$$IAE = \int_0^T |e(t)| dt \tag{35}$$

$$ISE = \int_0^T [e(t)]^2 dt \tag{36}$$

$$ITAE = \int_0^T t \cdot |e(t)|\, dt \tag{37}$$

$$ITSE = \int_0^T t \cdot [e(t)]^2\, dt \tag{38}$$

The performance standards mentioned act as fitness functions. The goal is to find values that minimize these requirements, resulting in optimal control performance. GAs are optimization algorithms that are inspired by natural selection and genetics. They are used to find the best settings for minimizing the desired performance requirements. This technique is repeatedly used to refine a population parameter setting using selection, crossover, and mutation operations until it converges on a solution that represents optimum tuning for the given system [53].

To fulfil the requirements of the PID control, the mathematical formulation of the fitness function is delineated as in Ref. [54]. The fitness function is designed to address the requirements of PID control through a multifaceted approach. It integrates the absolute value of the system deviation, denoted as e(t), employing a specific proportional operation with a coefficient to accommodate diverse emphasis control schemes. Additionally, the fitness function includes the current control input, u(t), incorporating the square of the input as a factor and subjecting this component to a proportional operation with a designated coefficient. Furthermore, the fitness function considers the system's rise time, denoted as t(u), and undergoes proportional calculation using a specified coefficient. In the presence of system overshoot, the fitness function considers overshoot a crucial element, implementing a relatively substantial scale factor as a penalty function to mitigate overshoot effectively. Considering the aspects mentioned above, the objective function of the system can be derived as follows:

$$\text{If } ey(t) \geq 0 \tag{39}$$

$$s = \int_0^\infty \left(w_1|e(t)| + w_2 u^2(t) \right) d(t) + w_3 \cdot t(u) \tag{40}$$

$$\text{If } ey(t) < 0 \tag{41}$$

$$s = \int_0^\infty \left(w_1|e(t)| + w_2 u^2(t) + w_4|ey(t)| \right) d(t) + w_3 \cdot t(u) \tag{42}$$

In the given context, where $ey(t)$ is defined as the difference between the current output y(t) and the previous output $y_{(t-1)}$, with y(t) representing the output, the fitness function is configured as the inverse of the objective function. Thus, the fitness function is expressed as $s = \frac{1}{s}$.

According to [55], using a PID control for motor control to minimize the rise time, the proportional gain is employed, while the derivative gain is utilized to reduce overshoot and hasten the settling time. The integral gain is applied to sustain the error at a minimal level. This approach facilitates the optimization of gains for enhanced response speed. Based on the studies in Refs. [56,57], PID controllers are adapted to handle a recognized class of plants due to their capability to exhibit favorable dynamics in response to set-point adjustments. Additionally, they demonstrate zero asymptotic error in the presence of constant disturbance inputs, including those added to the plant's input. Figure 8 shows the flowchart used for the GA.

Figure 9a shows the torque and power curves when the engine torque and speed are 400 Nm and 7000 rpm, respectively. Meanwhile, Figure 9b shows the fuel consumption map when the engine torque and speed are 400 Nm and 6000 rpm, respectively.
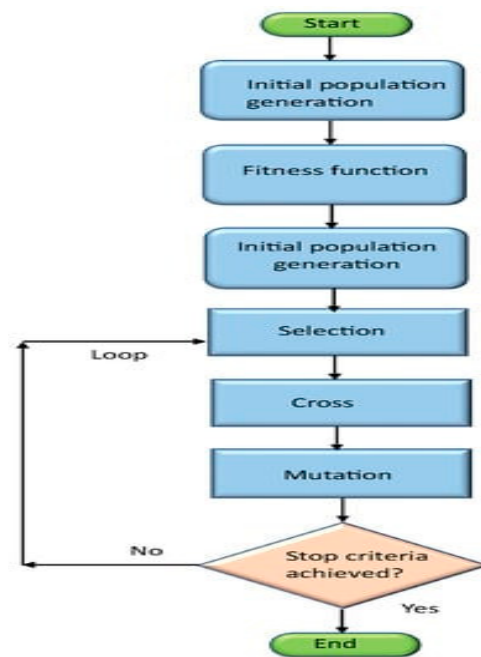
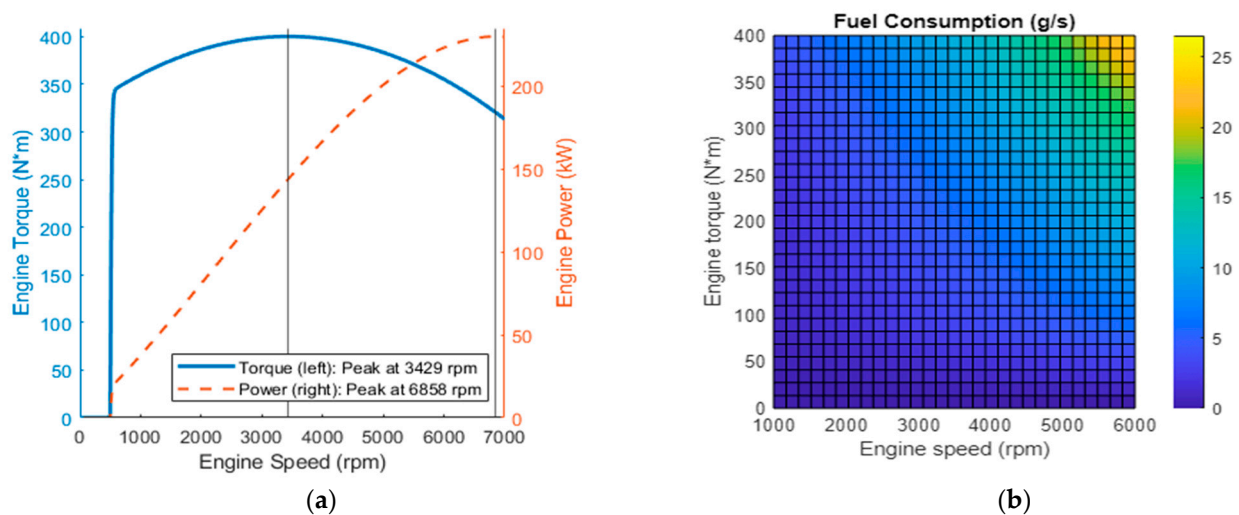**Figure 8.** Genetic algorithm flowchart [58].

(**a**)   (**b**)

Figure 9. (**a**) Plot of the torque and power curves when the engine torque is plotted against the engine speed. (**b**) Heat plot of the fuel consumption when the engine torque is plotted against the engine speed [41].

4. VCDS Software Test Setup

VCDS (VAG-COM Diagnostic System) is a software program used for VW Group (VAG) vehicle diagnostics and customization. VAG covers the Volkswagen Group, such as VAS and ODIS [59]. VCDS enables us to access and interact with numerous control modules in the vehicle's electronic systems, assisting us with diagnosing problems, performing code modifications, and accessing real-time data from sensors and modules. It can generate precise measurements that may be saved and exported to a computer as Comma-Separated Values (CSV) files that can be used for additional analysis and processing [60]. As a result, utilizing the diagnostics tool's previously indicated capability, an assortment of real-time measurements were collected, enabling the estimation of engine power output in real time. Regarding the data collected during on-road testing, the primary objectives involve validating the diagnostic tool's accuracy and forming a database necessary for developing the suggested hybrid powertrain. The VCDS software is utilized to obtain

fundamental car powertrain information via onboard diagnostics (OBD) [60,61]. Within the VCDS graphical user interface, a diverse array of functions are accessible from the main menu. These functionalities include automated scans of electronic controllers for diagnostic purposes, access to various installed electronic modules, service alert timeframe resets, and connectivity verification with the vehicle, among others.

As mentioned above, each menu branches into submenus, such as the "Select" menu, which provides access to all electronic modules within the vehicle [61]. Selecting any of these submenus enables users to retrieve fault codes, perform adjustments to system components, and, significantly for this undertaking, obtain real-time measurements of diverse parameters. A critical feature is the ability to conduct real-time measurements for these modules, with the option to store and export the data to a computer in CSV (Comma-Separated Values) format. This export capability facilitates subsequent interpretation and further data processing. Consequently, the diagnostic tool's functionalities were leveraged to undertake a series of real-time measurements, enabling the computation of real-time engine power output. This dataset was subsequently used to compare the simulated hybrid vehicle and the actual vehicle. The setup used is illustrated in Figure 10a. Figure 10b shows the data collection from the real car using the VCDS software. Only the essential data that would be used as the basis for the hybrid vehicle design were collected during the measurement, as visualized in the Results section.
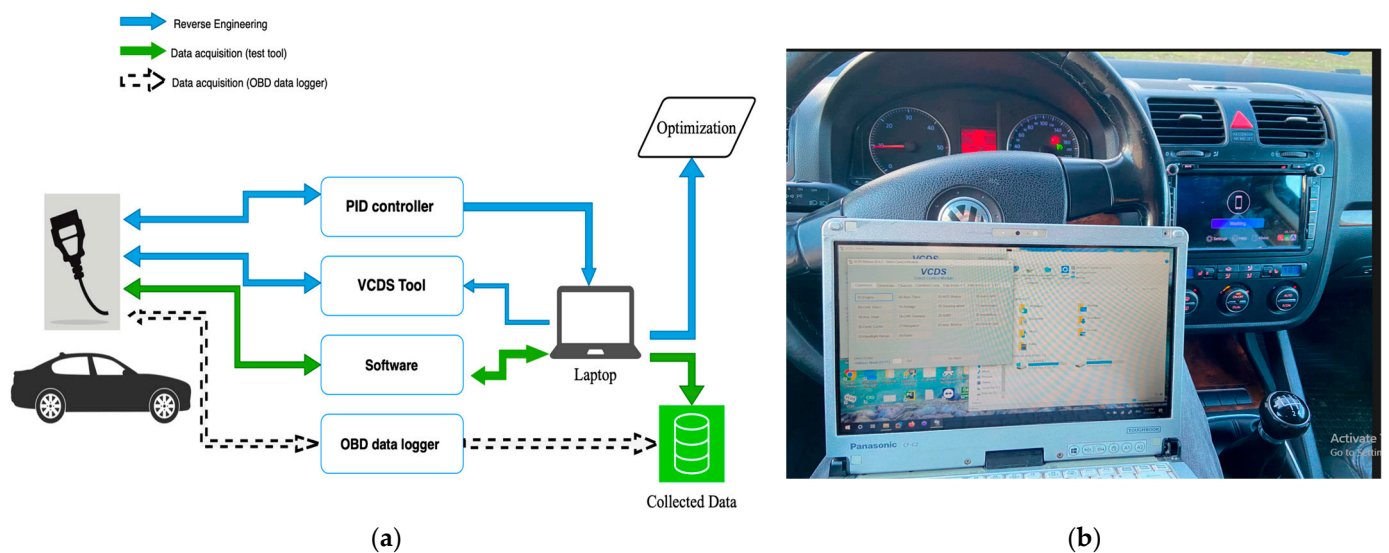

(**a**)　　　　　　　　　　　　　　　　　　　(**b**)

Figure 10. (**a**) Setup for data collection using VCDS. (**b**) Real measurements from the car.

5. MATLAB Models

The conventional vehicle was designed with a five-speed gearbox, which is required to determine how the engine's robustness transferred to the wheels. In the gearbox, a gearbox controller is utilized to guarantee control over gear selection and shifting. In addition to a throttle controller that controls the vehicle's operation, this component controls the flow of fuel and air to the engine, allowing for quick acceleration and deceleration, which is required for an accurate driving simulation. The engine and the electric motor were coupled to propel the vehicle for the hybrid model. The method of modeling the car was adopted from [62]. Figures 11 and 12 show the MATLAB models of the proposed vehicle.
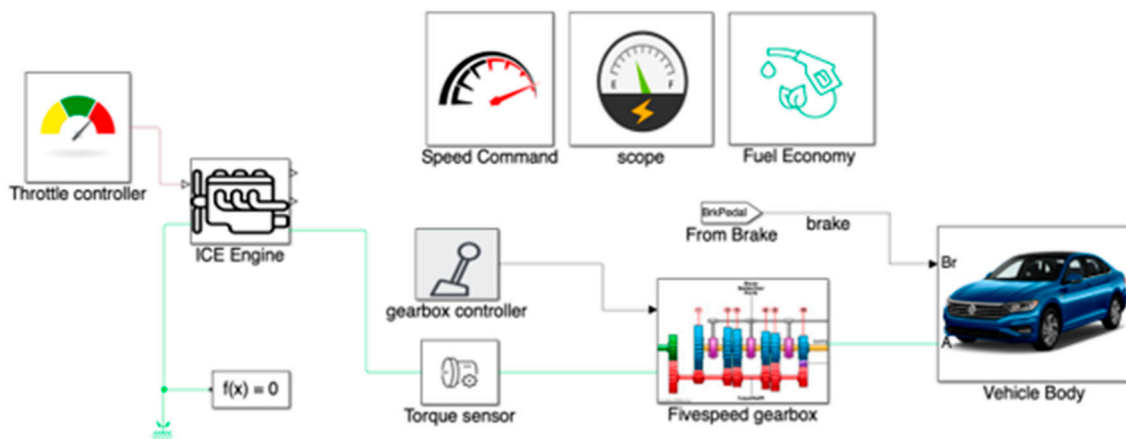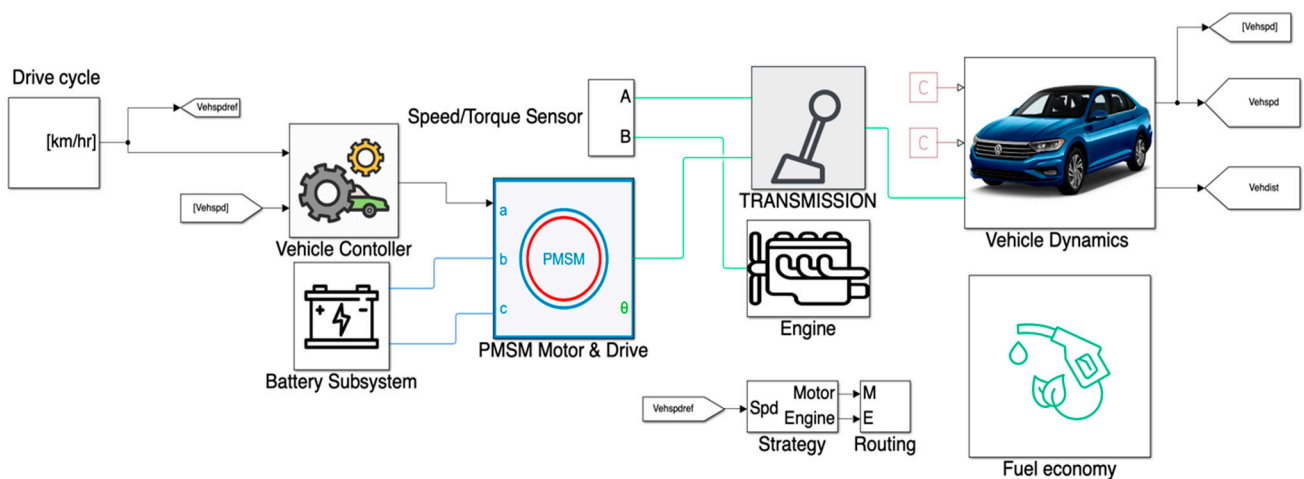
Figure 11. Conventional MATLAB model.

Figure 12. Parallel hybrid powertrain MATLAB model.

6. Simulation and Experimental Results

The results from the hybrid vehicle use the manual tuning of the PID controller with values depicted in Table 7, with the operating motor torque set to a continuous operation value of 400 Nm, shown in Figure 13a. In general, more continuous operating torque translates into superior acceleration performance. If swift acceleration is a priority for the vehicle, increased torque could help with dynamic performance. Higher torque can contribute to more effective energy recovery when braking if the car uses regenerative braking. This has the potential to improve the total energy efficiency, considering the vehicle's typical driving scenarios and usage trends. A higher torque may be advantageous for city driving with frequent stops and starts, whereas a lower torque may be suitable for highway cruising. On the other hand, the GA showed a reading very similar to the manual tuning regarding motor torque. Figure 13b shows that the vehicle travelled a distance of 1 km.

Table 7. PID parameters based on manual tuning.

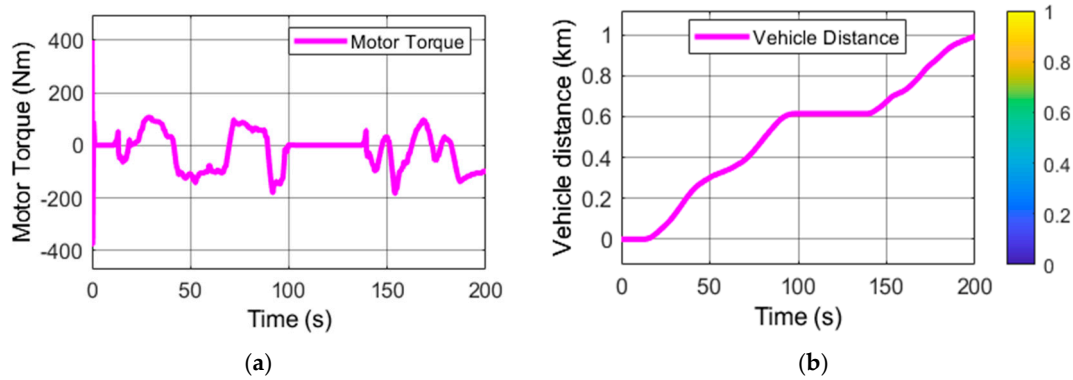| PID Parameters	Value
Kp	154
Ki	502
Kd	12

(a) (b)

Figure 13. (**a**) Motor torque during the 200 s simulation. The positive and negative account for the motoring and generating action of the PMSM. (**b**) Vehicle distance during the 200 s simulation with color to indicate the maximum distance covered (1 km).

Considering that the battery reached a State of Charge (SOC) of 99.75%, indicating near-full charge, the operational temperature managed by the battery management system was disregarded. Figure 14a illustrates the current of the battery. Figure 14b shows the battery SOC. During acceleration, the battery pulls a peak current of 116 A, and during deceleration, it experiences a minimum current of −73 A.
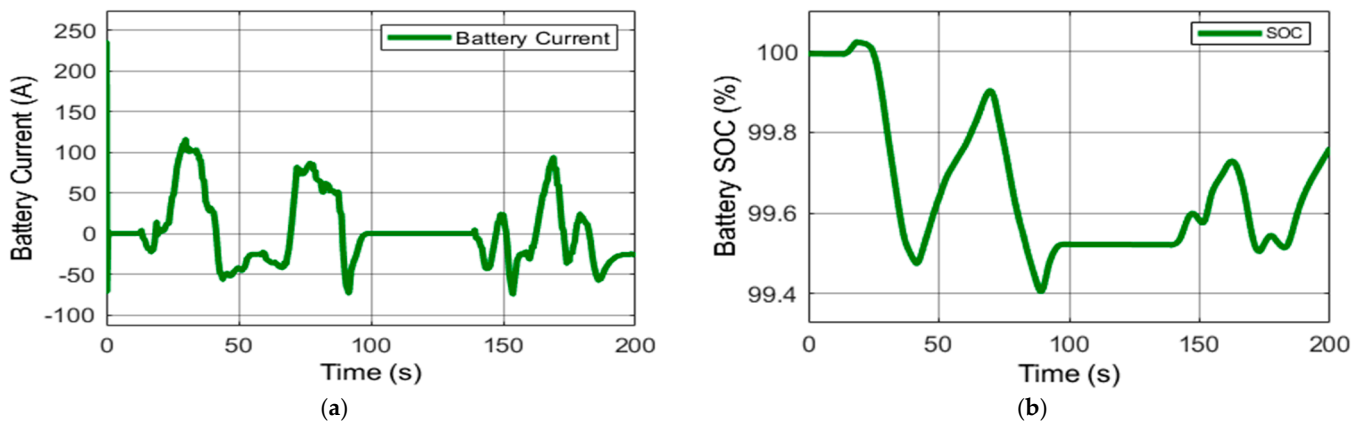

(a) (b)

Figure 14. (a) Current of the battery pack at 200 s. (b) Battery state of charge.

The battery can deliver more than 90 kW of power, with the vehicle utilizing 41 kW of that power at the vehicle's maximum speed, as depicted in Figure 15d, and the motor's consumed power of 37 kW. Moreover, the kilowatt-hour (kWh) utilization of the motor and battery's energy were 0.1177 kWh and 0.1307 kWh, respectively, as shown in Figure 15a. Furthermore, the total energies per 100 km for the motor and battery were approximately 11.8 kWh/100 km and 13.1 kWh/100 km, respectively. The genetic algorithm showed a reading similar to the manual tuning concerning motor battery power. Most real electric cars consume around 15 kWh for 100 km. The distinction observed in the graphs in Figure 15a indicates the energy dissipated from the battery to the PMSM. Since $E_b = 0.1307$ kWh represents the electrical energy utilized by the battery, and $E_m = 0.1177$ kWh is the mechanical energy used by the PMSM motor, the calculated energy efficiency (η) is as follows:

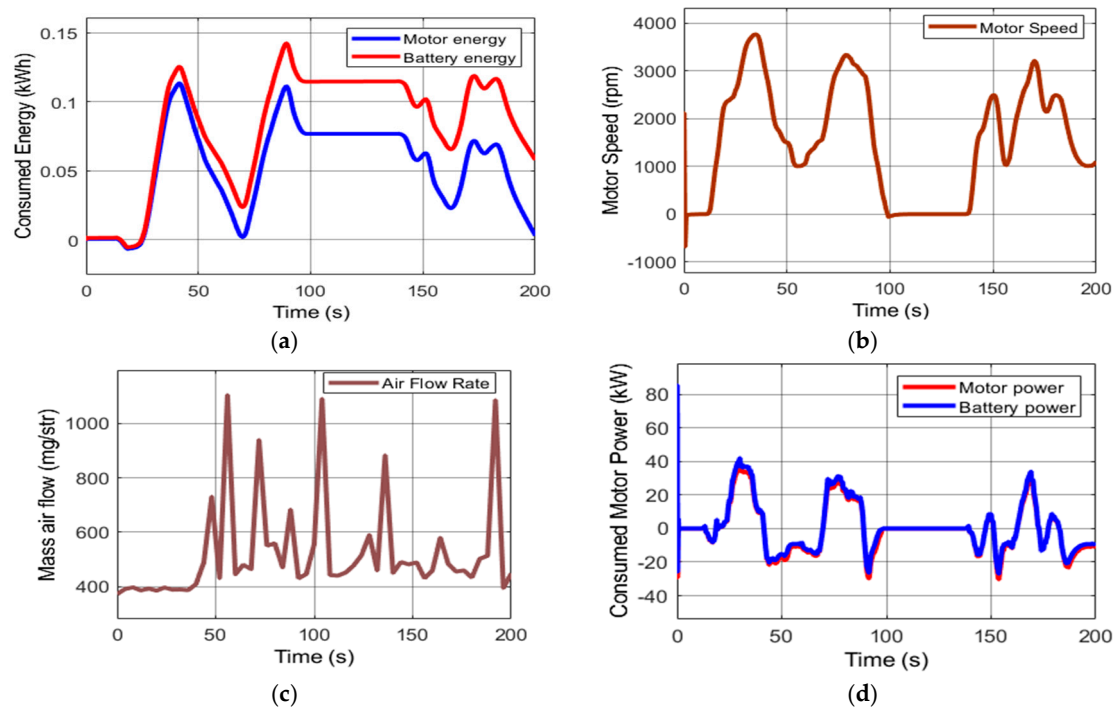$$\eta = \frac{E_m}{E_b} = \frac{0.1177}{0.1307} \times 100 = 90.05\% \tag{43}$$

Figure 15. (**a**) PMSM and battery energy consumption of the vehicle during the 200s simulation, where the red line represents the battery energy, and the blue line represents the motor energy. (**b**) PMSM motor operational speed. (**c**) Measured mass air standing at 450 mg/stroke during 200 s. (**d**) PMSM power and battery power consumption during the 200 s driving cycle, where the blue line represents the battery power, and the red line represents the motor power.

The motor's operational speed is 3770 rpm, which precisely mirrors the real-time velocity and is visually represented in Figure 15b. Simultaneously, Figure 15c shows the measured mass air flow (MAF) collected from the real car to measure the corresponding fuel consumption and compare it with simulated results. To scrutinize losses, one can analyze the energy transmission from the storage unit—specifically, from the car's battery to its wheels.

The following best GA-PID parameters, as presented in Table 8, were iteratively obtained with the help of the GA method. The signal input is used as the speed reference, and the output signal is the vehicle's actual speed.

Table 8. GA-PID parameters.

PID Parameters	Value
Kp	117.6
Ki	41.887
Kd	1.6762

Figure 16 exhibits the vehicle's real-time speed vs. the vehicle reference speed utilized from the WLTP speed command. The vehicle speed has successfully followed the reference with little oscillations detected; the duration included a 200 s time frame and 1 km distance.

Table 9 shows further information about fuel efficiency, obtained by reading the engine speed and torque and converting these using the fuel consumption table block, which conducts 1D linear interpolation of input values using the supplied table. The control mechanism that estimates fuel consumption based on diesel density and other criteria is then passed to the determined fuel economy function block. The analysis used in modeling the vehicle characteristics is based on the vehicle dynamics described in Figure 1 indicating

the forces acting on the vehicle body as presented in equations 1-5. While the parameters used in the simulation model are presented in Table 2.
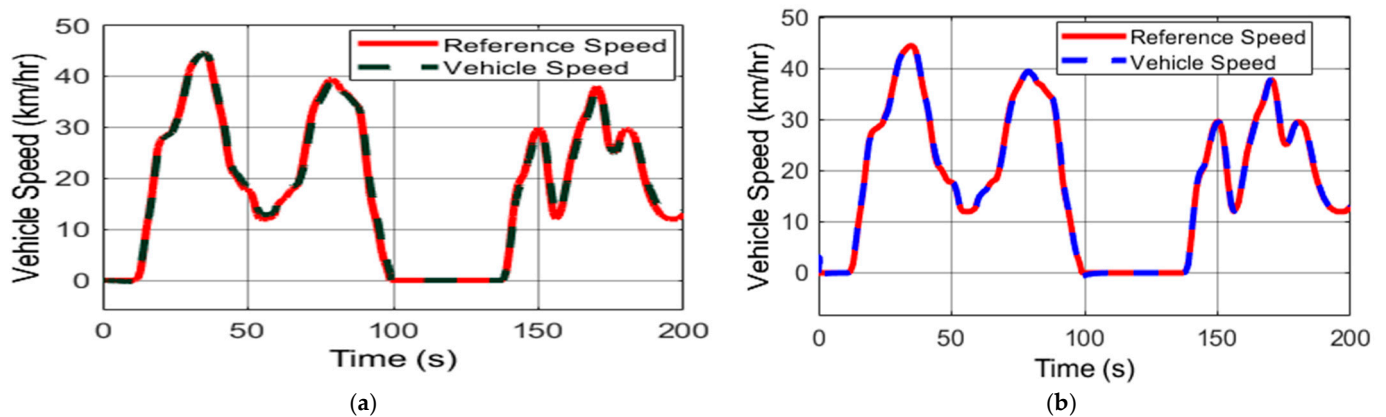

(**a**)

(**b**)

Figure 16. (**a**) Conventional vehicle's actual speed in blue line and reference speed in red dotted line controlled by a PI controller for the drive cycle of 200 s. (**b**) GA-PID-controlled reference speed and actual vehicle speed, where the red dotted line represents the reference speed, and the blue dotted line represents the vehicle's actual speed for the whole duration of the drive cycle. The WLTP test procedure was adopted from Ref. [63].

Table 9. Fuel economy of the conventional vehicle and HEV vehicles.

Parameters	ICE Usage	HEV Usage
Liter/100 kilometer [L/100 km]	8.061	0.8499
Kilometer/liter [km/L]	12.41	117.7
Miles per gallon [MPG]	29.18	276.8
Total fuel used [L]	0.08049	0.008447

7. Discussion

This research involves transforming a conventional MK5 vehicle into a HEV using a PMSM and Nissan Leaf battery pack traction system. The aim was to evaluate the fuel economy, energy consumption, and controller performance of both cars and to decide whether converting the MK5 Jetta from conventional to hybrid is useful in terms of the optimal fuel economy. Figures 13–20 show the simulation and experimental results. Table 9 presents this research's simulated fuel consumption for the conventional and hybrid powertrain. The WLTP was used in the test procedure, since it closely relates to real-world driving scenarios. The study in [64] states that on-road and laboratory testing is critical to ensuring adequate performance.
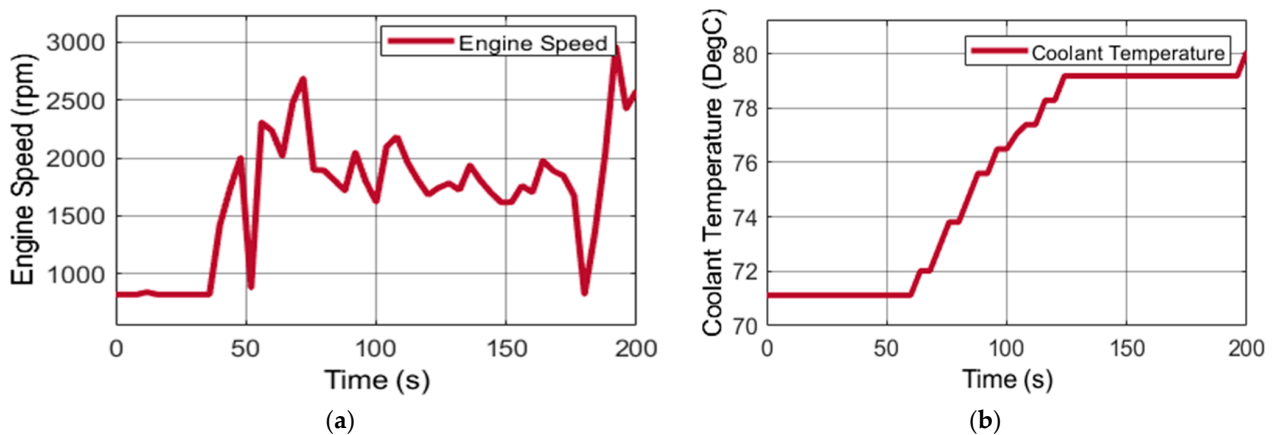

(**a**)

(**b**)

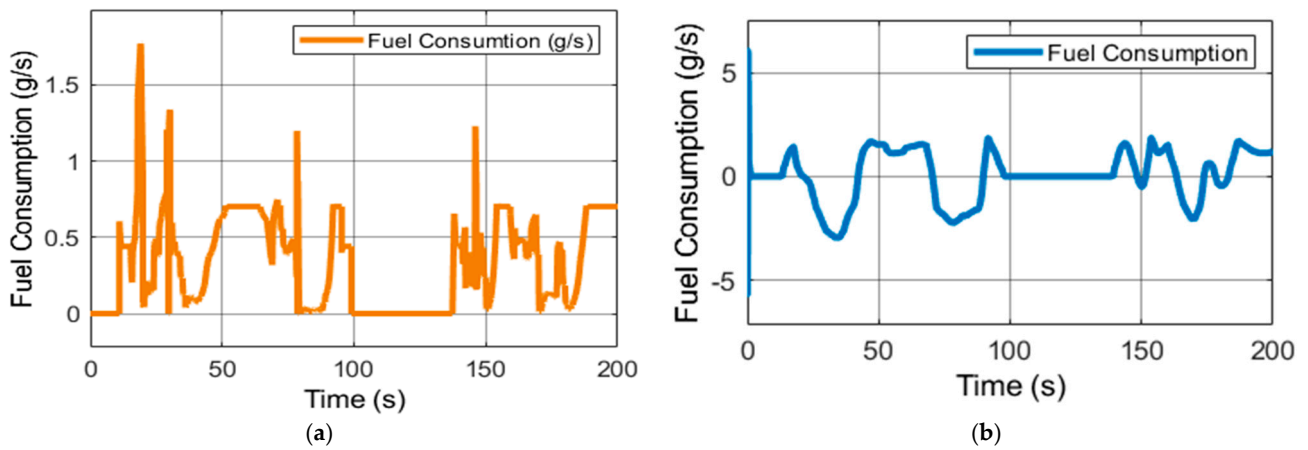**Figure 17.** (**a**) ICE-measured speed at 200 s. (**b**) ICE coolant temperature measured for about 200 s.

Figure 18. Divergence in vehicular fuel efficiency is evident when contrasting the conventional vehicle's fuel consumption with that of the HEV. (**a**) Fuel economy of the conventional vehicle, which is equivalent to the fuel flow rate in g/s for the simulated car. (**b**) Fuel economy of the HEV, which is equivalent to the fuel flow rate in g/s for the simulated car.
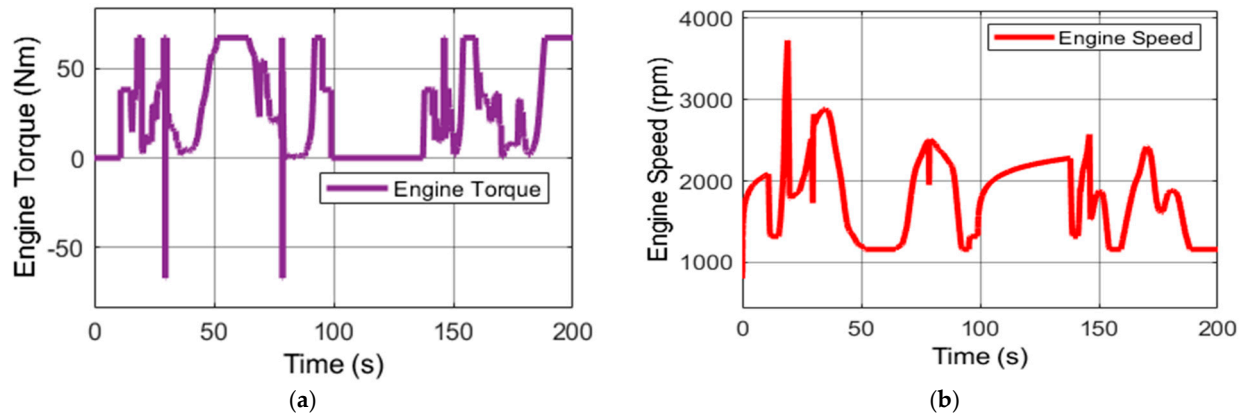

Figure 19. (**a**) ICE torque illustrates the torque delivery in the ICE. (**b**) Simulated speed of the diesel ICE.
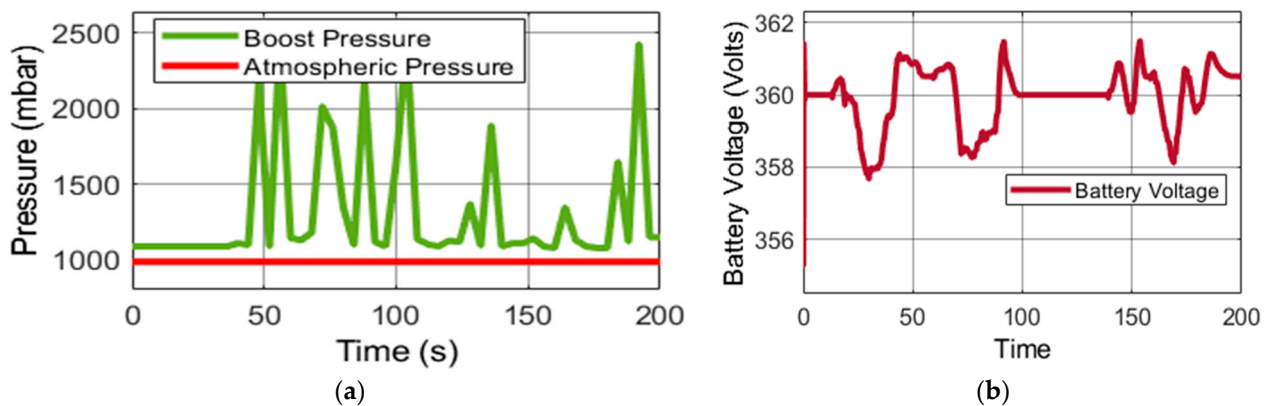

Figure 20. (**a**) Measured atmospheric and boost pressures. (**b**) Battery voltage.

Figure 16a,b show that the PID based on the GA could search the vehicle trajectory optimally. The car attained a maximum speed of 44 km/h in 200 s using the WLTP drive cycle. MATLAB simulations demonstrated the controller's effectiveness in tracking the vehicle trajectory using manual tuning for the PID controller, obtained by executing several tests until optimal improvements were attained. The final results are significant influencing

elements, necessitating accurate tuning of the control parameters from the speed reference with a steady state and low oscillations. Therefore, the energy efficiency of 90.05% was achieved irrespective of the transmission losses from the battery to the electric motor.

The system is subject to parameter uncertainty, nonlinearities, operating conditions such as stability, and sensor behavior blocks or components that replicate the real system's dynamic characteristics. These variables could significantly impact the controller's performance. A GA-PID controller was developed to solve these issues, and its settings were fine-tuned through a series of tests to achieve the best possible results. The system's stability was maintained through multiple iterations on the basis of decreasing the performance cost function or performance indices. These indices, such as the ISE, IAE, ITAE, and ITSE, were computed iteratively for the robustness of the system and disturbance rejection.

The average experimental fuel consumption was found to be in the range of 5.4 to 7.8 L/100 km. At the same time, for urban driving, it was found to be approximately 7 L/100 km. However, the Jetta MK5 vehicle was found to have excellent efficiency with a 1.4 16v FSI engine, consuming around 6.3 L/100 km, and for the 1.9 TDI, the fuel consumption was 5.2 L/100 KM. With a 2.0 TDI engine, the fuel consumption was found to be less for the VW Jetta manufactured between 2005 and 2008; However, the 1.4 L ICE was one of the most efficient engines [65]. However, in this research, the ICE-operated vehicle achieved 8.061 L/100 km fuel economy.

Meanwhile, fuel consumption was significantly reduced for the hybrid version of the car. The average fuel consumption of the hybrid vehicle was 0.8499 L/100 km based on the optimized PID controller. The fuel flow translated from these results is depicted in Figure 18. Figure 18a shows the simulated fuel flow rate of approximately 0.61 g/s at 1200 rpm of the ICE for the conventional car, and Figure 18b shows the fuel flow rate of about 1.1 g/s at 1000 rpm of the motor and 1200 rpm of the ICE for the hybrid vehicle. The values of the fuel consumption at these speeds are practically considered to be at an idle state or partially opened throttle conditions. In this situation, the fuel flow in the hybrid was higher than that of conventional cars. However, at some point, the hybrid fuel flow was 0.2 g/s, and the flow for the traditional vehicle was 0.41 g/s, respectively. This fuel consumption was not constant due to the motoring and generating action of the motor in the hybrid vehicle; therefore, the fuel economy was assessed cumulatively using MATLAB in L/100 km. Similarly, the consumption efficiency should be interpreted from the calculated cumulative fuel economy studied in Ref. [66].

For the measurement from the real car, the mass air flow, as shown in Figure 15c, was collected, which was found to be 450 mg/stroke converted to 57.17 g/s at 2541 rpm for an ICE speed at 200 s (translating to air flow of 27 g/s at 1200 rpm ICE speed for 200 s). However, the engine's air fuel ratio (AFR) is 14.5, which showed the measured fuel flow of the real car to be 1.86 g/s. The fuel flow from the real measurement was found to be 9.48 g/s for a mass air flow of 1100 mg/stroke. Practically, considering the environmental conditions and other external factors, this fuel flow is acceptable and could provide the required fuel economy for a real car. Figures 17a and 19b show the experimental and simulated ICE speeds, respectively. The experimental speed was measured to be around 3000 rpm, and the simulated speed was about 3700 rpm, which shows that the simulated car required less torque than the real car in the case of the engine. As shown in Figure 15b, the motor had a speed of 3770 rpm. Therefore, the combined motor and engine torque would be suitable for highways, where more torque is required.

This is obvious, as can be seen from Figures 13a and 19a, which show the motor and engine torques, respectively. The combined motor and engine torques were translated into the vehicle movement in the hybrid vehicle configuration. Figure 15a,d show the energy and power consumption of the hybrid powertrain. The little space between battery and motor energy or power was due to the energy transmission losses from the battery to the electric motor. The energy and power consumption showcased an optimized efficiency of over 90% for the powertrain. Figure 20a shows the experimental boost and atmospheric pressures, and Figure 20b shows the battery voltage for the Nissan Leaf battery pack. The

maximum voltage of the pack is 403.2 V, with each cell having 4.2 V. The used voltage was around 361.5 V. In practice, this voltage would not be less than 250 V.

Moreover, boost pressure minus the atmospheric pressure gives the actual boost pressure. According to Figure 20a, the boost pressure was around 1100 mbar to 2400 mbar, and the atmospheric pressure was about 1000 mbar according to the measurement. Therefore, the actual boost pressure was approximately 1.3 bar. This was enough pressure. This shows that the turbo geometry moving mechanism was not faulty and was not stuck in one place. The estimated theoretical pressure was around 1.2 bar at the engine speed of 2541 rpm in Figure 17a.

8. Conclusions

The dangerous emissions from ICE-powered vehicles have been a global chronic concern, and the short range of operation attributed to EVs is undesirable. Therefore, this research proposes a simple design method taking into consideration the model complexity level for the hybrid powertrain of the VW Jetta MK5 vehicle to meet the desired long-range demand and reduce the fuel consumed by its conventional counterpart. Moreover, this article replaces the 1.9 TDI PD engine, introducing a more recent technology, a 2.0 L TDI CR compression ignition (CI) engine, which complies with the EU6d exhaust emission standard, with a CR fuel system for an older-version VW Jetta MK5, capable of producing a peak power of 80 kW, along with a 2011 Nissan Leaf battery with 24 kWh nominal capacity (allowing 80% DOD rate) coupled with a Parker PMSM motor (103 kW peak power). This system reduced the fuel consumption to 2.664 L/100 km compared to the conventional car, which consumed 6.624 L/100 km. The 2.0 TDI CR has improved fuel delivery and volumetric efficiency, because it uses more valves. Therefore, this research utilizes a mathematical framework defining the vehicle and WLTP real-world test profile to conduct an optimum control design. The 2.0 engine may have good fuel economy, but this research also proposed an enhanced PID controller on the basis of an artificially intelligent GA to tune the controller parameters to account for the system's complexity and for optimal fuel economy versus the traditional 1.9 TDI ICE technology.

The proposed control system in this research consists of two methods: control of the MK5 vehicle operating through the ICE only and control of the transformed hybrid version of the proposed car. Both control methods were designed to meet the demand for fast response and robustness and to reduce the cost of the practical implementation, considering the model's complexity and the technical differences. The GA has been used in this article to iteratively compute the optimal gains on the basis of the desired vehicle's trajectory of the proposed controller to improve its robustness against model uncertainties and external disturbances. As a result, the controller has less computational cost and is easy and useful for practical implementation for industrial and commercial mechatronic products, especially for energy and fuel technology in powertrain electrification.

The enhanced GA-PID was developed to meet the system's monitoring durability, parametric uncertainty, and disturbances. The research leverages the conventional VW car characteristics and creates a hybrid version, introducing a Parker PMSM electrical machine to reduce the fuel consumption of the traditional gas-powered Jetta MK5 vehicle. To validate the controller's performance, it was applied to a dynamic model of the vehicle with an actuator (engine) in the case of the conventional vehicle and the motor and engine actuators in the case of the hybrid powertrain and other external disturbances. Therefore, the simulation results demonstrate the controller's desirable tracking accuracy as it consumes significantly less fuel with both manual and GA tunning techniques. The controller indicates an excellent tracking ability in finite time, eliminating the effect of model uncertainty and providing the desired speed command.

A commonly used data collection method (VCDS unit) was employed as a framework for a performance comparison to demonstrate the superiority of our design approach. The software test rig platform has been set up for the data collection based on real time. The measured data were used as the basis for designing the hybrid powertrain. The designed car

had significantly improved fuel consumption compared to the fuel consumption obtained from the actual measurement. The successful conversion of the VW Jetta MK5 into a hybrid powertrain showcased the capabilities of PMSM motors and batteries and the advanced software capability for transitioning conventional vehicles into HEVs. The methodologies used and the outcomes obtained pave the way for further advancements in developing and optimizing hybrid powertrains. In this research, the hybrid powertrain reduced fuel consumption by 89.46% compared to a traditional ICE car and achieved an energy efficiency of 90.05%. Future research developments should consider this vehicle's real transformation and establish an online CAN bus communication protocol for effective performance monitoring and data analysis.

Moreover, adopting Lyapunov's theory should prove the system's general stability. The real measurement results from the conventional car can be leveraged through system identification for optimal design and performance. In addition, the gear ratios should be optimized based on the theoretical formulations introduced in Section 2.5.

References

1. Venditti, M. Analysis of the Performance of Different Machine Learning Techniques for the Definition of Rule-based Control Strategies in a Parallel HEV. *Energy Procedia* **2016**, *101*, 685–692. [CrossRef]
2. D'ambrosio, S.; Di Dio, C.; Finesso, R. Model-Based Calibration and Control of Tailpipe Nitrogen Oxide Emissions in a Light-Duty Diesel Engine and Its Assessment through Model-In-The-Loop. *Energies* **2023**, *16*, 8030. [CrossRef]
3. Ehsani, M.; Gao, Y.; Longo, S.; Ebrahimi, K. *Modern Electric, Hybrid Electric, and Fuel Cell Vehicles*, 3rd ed.; Taylor & Francis Group, LLC: Boca Raton, FL, USA, 2018; Volume 3.
4. Lai, L.A. *Development of Design and Control Methodology for Next Generation Parallel Hybrid Electric Vehicle*; Texas A&M University: College Station, TX, USA, 2012.
5. Berjoza, V.P. Investigation in fuel consumption of a hybrid and conventional vehicle. *Agron. Res.* **2020**, *18*, 1027–1035. [CrossRef]
6. Ventura, L.; Finesso, R.; Malan, S.A. Development of a Model-Based Coordinated Air-Fuel Controller for a 3.0 dm^3 Diesel Engine and Its Assessment through Model-in-the-Loop. *Energies* **2023**, *16*, 907. [CrossRef]
7. D'Agati, L.; Benomar, Z.; Longo, F.; Merlino, G.; Puliafito, A.; Tricomi, G. IoT/Cloud-Powered Crowdsourced Mobility Services for Green Smart Cities. In Proceedings of the 2021 IEEE 20th International Symposium on Network Computing and Applications (NCA), Boston, MA, USA, 23–26 November 2021; pp. 1–8. [CrossRef]
8. Stamadianos, T.; Kyriakakis, N.A.; Marinaki, M.; Marinakis, Y. Routing Problems with Electric and Autonomous Vehicles: Review and Potential for Future Research. *SN Oper. Res. Forum* **2023**, *4*, 46. [CrossRef]
9. Iodice, P.; Amoresano, A.; Langella, G.; Marra, F.S. Numerical Optimization and Energetic Advantages of an Innovative Solar Power System Based on Scheffler Receiver Coupled with Volumetric Expanders. *Energy Environ.* **2022**, *34*, 602–620. [CrossRef]
10. Hata, R.; Isojima, S. The Road to Liquid Hydrogen Electric Vehicle Powered by High-Temperature Superconducting Motor—Utilizing Tank Trucks to Deliver LH2. *SEI Tech. Rev.* **2009**, *69*, 25–35.

11. Oh, S.; Park, J. Numerical Prediction on In-Cylinder Mixture Formation and Combustion Characteristics for SIDI Engine Fueled with Hydrogen: Effect of Injection Angle and Equivalence Ratio. *Energies* **2023**, *16*, 7509. [CrossRef]

12. Bisht, P.; Yadav, J. Optimal Speed Control of Hybrid Electric Vehicle Using GWO Based Fuzzy-PID Controller. In Proceedings of the 2020 International Conference on Advances in Computing, Communication & Materials (ICACCM), Dehradun, India, 21–22 August 2020; pp. 115–120. [CrossRef]

13. Baz, R.; El Majdoub, K.; Giri, F.; Taouni, A. Self-tuning fuzzy PID speed controller for quarter electric vehicle driven by In-wheel BLDC motor and Pacejka's tire model. *IFAC-PapersOnLine* **2022**, *55*, 598–603. [CrossRef]

14. Saeks, R.; Cox, C.; Neidhoefer, J.; Mays, P.; Murray, J. Adaptive control of a hybrid electric vehicle. *IEEE Trans. Intell. Transp. Syst.* **2002**, *3*, 213–234. [CrossRef]

15. Zhou, Q.; Du, C. A quantitative analysis of model predictive control as energy management strategy for hybrid electric vehicles: A review. *Energy Rep.* **2021**, *7*, 6733–6755. [CrossRef]

16. Schouten, N.; Salman, M.; Kheir, N. Fuzzy logic control for parallel hybrid vehicles. *IEEE Trans. Control Syst. Technol.* **2002**, *10*, 460–468. [CrossRef]

17. Maaruf, M.; Hamanah, W.M.; Abido, M.A. Hybrid Backstepping Control of a Quadrotor Using a Radial Basis Function Neural Network. *Mathematics* **2023**, *11*, 991. [CrossRef]

18. George, M.A.; Kamat, D.V.; Kurian, C.P. Electronically Tunable ACO Based Fuzzy FOPID Controller for Effective Speed Control of Electric Vehicle. *IEEE Access* **2021**, *9*, 73392–73412. [CrossRef]

19. Zhang, Y.; Chen, Z.; Li, G.; Liu, Y.; Chen, H.; Cunningham, G.; Early, J. Machine Learning-Based Vehicle Model Construction and Validation—Toward Optimal Control Strategy Development for Plug-In Hybrid Electric Vehicles. *IEEE Trans. Transp. Electrif.* **2021**, *8*, 1590–1603. [CrossRef]

20. Korkmaz, M.; Aydogdu, O.; Dogan, H. Design and performance comparison of variable parameter nonlinear PID controller and genetic algorithm based PID controller. In Proceedings of the 2012 International Symposium on Innovations in Intelligent Systems and Applications (INISTA), Trabzon, Turkey, 2–4 July 2012; pp. 1–5. [CrossRef]

21. Lü, X.; Wu, Y.; Lian, J.; Zhang, Y.; Chen, C.; Wang, P.; Meng, L. Energy management of hybrid electric vehicles: A review of energy optimization of fuel cell hybrid power system based on genetic algorithm. *Energy Convers. Manag.* **2020**, *205*, 112474. [CrossRef]

22. Wikipedia. Available online: https://en.wikipedia.org/wiki/Volkswagen_Jetta_(A5)#cite_note-3 (accessed on 10 January 2024).

23. Auto-Data.net. Available online: https://www.car.info/en-se/volkswagen/jetta/a5-typ-1k-52785/specs (accessed on 3 January 2024).

24. Bodzás, S.; Tiba, Z.; Ailer, P.; Husi, G. Redesign of a Volkswagen Crafter vehicle to a hybrid vehicle having e-motor and diesel engine. *IOP Conf. Ser. Mater. Sci. Eng.* **2022**, *1237*, 012008. [CrossRef]

25. Abe, M. Fundamentals of Vehicle Dynamics. In *Vehicle Handling Dynamics*, 2nd ed.; Elsevier: Amsterdam, The Netherlands, 2015; pp. 45–107. [CrossRef]

26. Yang, S.; Lu, Y.; Li, S. An overview on vehicle dynamics. *Int. J. Dyn. Control* **2013**, *1*, 385–395. [CrossRef]

27. Zhang, W. Dynamics of Coupled Systems in High-Speed Railways Theory and Practice. In *Dynamics of Coupled Systems in High-Speed Railways*; Zhang, W., Ed.; Elsevier: Amsterdam, The Netherlands, 2020; pp. 1–54. [CrossRef]

28. Babangida, A.; Szemes, P.T. Electric Vehicle Modelling and Simulation of a Light Commercial Vehicle Using PMSM Propulsion. *Hung. J. Ind. Chem.* **2021**, *49*, 37–46. [CrossRef]

29. Iodice, P.; Fornaro, E.; Cardone, M. Hybrid Propulsion in SI Engines for New Generation Motorcycles: A Numerical-Experimental Approach to Assess Power Requirements and Emission Performance. *Energies* **2022**, *15*, 6312. [CrossRef]

30. Zhang, F.; Wang, L.; Coskun, S.; Pang, H.; Cui, Y.; Xi, J. Energy Management Strategies for Hybrid Electric Vehicles: Review, Classification, Comparison, and Outlook. *Energies* **2020**, *13*, 3352. [CrossRef]

31. Miller, J.M. *Propulsion Systems for Hybrid Vehicles*; British Library Cataloguing in Publication Data: London, UK, 2008; Volume 45.

32. Babangida, A.; Szemes, P.T. Electric Vehicle Modeling and Simulation of Volkswagen Crafter with 2.0 TDI CR Diesel Engine VW Vehicle 2020 Based PMSM Propulsion. *Recent Innov. Mechatron.* **2021**, *8*, 1–6.

33. Zou, J.F.Y.; Zhang, X. Quantifying Electric Vehicle Battery's Ohmic Resistance Increase Caused by Degradation from on-board Data. *IFAC-PapersOnLine* **2019**, *52*, 297–302. [CrossRef]

34. Adams Intelligence. The Average Battery Size of Plug-in-Hybrids is Soaring. Available online: https://www.adamasintel.com/ev-increase-battery-capacity-average-kwh-phev-up-27-percent (accessed on 5 February 2024).

35. Melkebeek, J.A. *Electrical Machines and Drives Fundamentals and Advanced Modelling*; Springer: Cham, Switzerland, 2018. [CrossRef]

36. Szalay, I.; Kohlrusz, G.; Fodor, D. Modeling of slotless surface-mounted PM synchronous motor for sensorless applications. In Proceedings of the 2014 IEEE International Electric Vehicle Conference (IEVC), Florence, Italy, 17–19 December 2014; pp. 1–5. [CrossRef]

37. Virani, V.P.; Arya, S.V.; Baria, J.C. Modelling and Control of PMSM Drive by Field Oriented Control For HEV. *Adv. Power Gener. Renew. Energy Sources* **2019**, 1–11. [CrossRef]

38. Car.info. Available online: https://www.car.info/en-se/volkswagen/jetta/jetta-4-door-20-tdi-8168709/specs (accessed on 3 January 2024).

39. Abdul, M.; Begh, W.; Herzog, H.-G. *Comparison of Field Oriented Control and Direct Torque Control*; Technische Universität München: Munich, Germany, 2018. [CrossRef]

40. Amin, F.; Bin Sulaiman, E.; Utomo, W.M.; Soomro, H.A.; Jenal, M.; Kumar, R. Modelling and Simulation of Field Oriented Control Based Permanent Magnet Synchronous Motor Drive System. *Indones. J. Electr. Eng. Comput. Sci.* **2017**, *6*, 387–395. [CrossRef]
41. Generic Internal Combustion Engine-MATLAB. Available online: https://www.mathworks.com/help/sdl/ref/genericengine.html (accessed on 5 January 2024).
42. Popa, G.; Gheți, M.A. Locomotive Diesel Engine Operation with Optimal Specific Fuel Consumption. *Procedia Manuf.* **2020**, *46*, 440–444. [CrossRef]
43. Ahssan, M.R.; Ektesabi, M.; Gorji, S. Gear Ratio Optimization along with a Novel Gearshift Scheduling Strategy for a Two-Speed Transmission System in Electric Vehicle. *Energies* **2020**, *13*, 5073. [CrossRef]
44. Oglieve, C.J.; Mohammadpour, M.; Rahnejat, H. Optimisation of the vehicle transmission and the gear-shifting strategy for the minimum fuel consumption and the minimum nitrogen oxide emissions. *Proc. Inst. Mech. Eng. Part D J. Automob. Eng.* **2017**, *231*, 883–899. [CrossRef]
45. Volkswagen Jetta (A5). Available online: https://en.wikipedia.org/wiki/Volkswagen_Jetta_(A5) (accessed on 10 January 2024).
46. Qin, Y.; Zhao, G.; Hua, Q.; Sun, L.; Nag, S. Multiobjective Genetic Algorithm-Based Optimization of PID Controller Parameters for Fuel Cell Voltage and Fuel Utilization. *Sustainability* **2019**, *11*, 3290. [CrossRef]
47. Dhieb, Y.; Yaich, M.; Guermazi, A.; Ghariani, M. PID Controller Tuning using Ant Colony Optimization for Induction Motor. *J. Electr. Syst.* **2019**, *15*, 133–141.
48. Elbayomy, K.M.; Zongxia, J.; Huaqing, Z. PID Controller Optimization by GA and Its Performances on the Elec-tro-hydraulic Servo Control System. *Chin. J. Aeronaut.* **2008**, *21*, 378–384. [CrossRef]
49. Pradana, A.; Haque, M.; Nadarajah, M. Control Strategies of Electric Vehicles Participating in Ancillary Services: A Comprehensive Review. *Energies* **2023**, *16*, 1782. [CrossRef]
50. Maghfiroh, H.; Nizam, M.; Praptodiyono, S. PID optimal control to reduce energy consumption in DC-drive system. *Int. J. Power Electron. Drive Syst.* **2020**, *11*, 2164–2172. [CrossRef]
51. Ibrahim, M.A.; Mahmood, A.K.; Sultan, N.S. Optimal PID controller of a brushless dc motor using genetic algorithm. *Int. J. Power Electron. Drive Syst.* **2018**, *10*, 822–830. [CrossRef]
52. Krohling, R.; Rey, J. Design of optimal disturbance rejection PID controllers using genetic algorithms. *IEEE Trans. Evol. Comput.* **2001**, *5*, 78–82. [CrossRef]
53. Mirzal, A.; Yoshii, S.; Furukawa, M. PID parameters optimization by using genetic algorithm. *ISTECS J.* **2006**, *8*.
54. Zhao, J.; Xi, M. Self-Tuning of PID Parameters Based on Adaptive Genetic Algorithm. *IOP Conf. Ser. Mater. Sci. Eng.* **2020**, *782*, 042028. [CrossRef]
55. Somwanshi, D.; Bundele, M.; Kumar, G.; Parashar, G. Comparison of Fuzzy-PID and PID Controller for Speed Control of DC Motor using LabVIEW. *Procedia Comput. Sci.* **2019**, *152*, 252–260. [CrossRef]
56. Precup, R.-E.; Preitl, S.; Tar, J.K.; Tomescu, M.L.; Takacs, M.; Korondi, P.; Baranyi, P. Fuzzy Control System Performance Enhancement by Iterative Learning Control. *IEEE Trans. Ind. Electron.* **2008**, *55*, 3461–3475. [CrossRef]
57. Precup, R.-E.; Preitl, S.; Korondi, P. Fuzzy Controllers with Maximum Sensitivity for Servosystems. *IEEE Ind. Electron. Mag.* **2007**, *54*, 1298–1310. [CrossRef]
58. Calvachi, D.; Tipán, L.; Jaramillo, M. Localization and Sizing of Distributed Generation through a Genetic Algorithm to Improve Voltage Profile Using Ecuadorian Standards. *Energies* **2023**, *16*, 4139. [CrossRef]
59. Ross-Tech. Ross-Tech. VAG-COM. Available online: https://www.ross-tech.com/vag-com/product.html (accessed on 10 October 2023).
60. Anton, B.; Florescu, A. Design and Development of Series-Hybrid Automotive Powertrains. *IEEE Access* **2020**, *8*, 226026–226041. [CrossRef]
61. Ross Tech. Current Version of VCDS®for customers with High- Tech HEX, KEY, KII or Micro-CAN Series Interfaces. Ross-Tech LLC. Available online: https://www.ross-tech.com/vcds/download/current.php (accessed on 12 October 2023).
62. Github.com. Available online: https://github.com/maybachy1121/Simscape-Powertrain-SI-Model/find/master (accessed on 10 December 2023).
63. Auger, D.J. Drive Cycle Simulink Block Model. Available online: https://www.mathworks.com/matlabcentral/fileexchange/46777-driving-cycle-simulink-block (accessed on 1 January 2024).
64. Jaworski, A.; Kuszewski, H.; Lew, K.; Wojewoda, P.; Balawender, K.; Woś, P.; Longwic, R.; Boichenko, S. Assessment of the Effect of Road Load on Energy Consumption and Exhaust Emissions of a Hybrid Vehicle in an Urban Road Driving Cycle—Comparison of Road and Chassis Dynamometer Tests. *Energies* **2023**, *16*, 5723. [CrossRef]
65. Volkswagen Jetta MK5. 2005. Available online: https://www.auto-abc.eu/Volkswagen-Jetta/g1285-2005 (accessed on 10 January 2024).
66. Balcı, Ö.; Karagöz, Y.; Gezer, O.; Kale, S.; Köten, H.; Pusat, S.; Yüksek, L. Numerical and experimental investigation of fuel consumption and CO_2 emission performance for a parallel hybrid vehicle. *Alex. Eng. J.* **2021**, *60*, 3649–3667. [CrossRef]